Multi scale image and multi scale deformation of brain anatomy for building average brain atlases

Colin Studholme, Valerie Cardenas, Michael Weiner

Dept. Radiology, UCSF, VAMC(116R), San Francisco, CA 94121

ABSTRACT

In this work we consider the process of aligning a set of anatomical MRI scans, from a group of subjects, to a single reference MRI scan as accurately as possible. A key requirement of this anatomical normalisation is the ability to bring into alignment brain images with different ages and disease states with equal accuracy and precision, enabling the unbiased comparison of different groups. Typical images of such anatomy may vary in terms of both tissue shape, location and contrast. To address this we have developed, a highly localised free-form inter-subject registration algorithm driven by normalised mutual information. This employs an efficient multi-image resolution and multi-deformation resolution registration procedure. In this paper we examine the behaviour of this algorithm when applied to aligning high-resolution MRI of groups of younger, older and atrophied brain anatomy to different target anatomies. To gain an insight into the quality of the spatial normalisation, we have examined two properties of the transformations: The residual intensity differences between spatially normalised MRI values and the spatial discrepancies in transformation estimates between group and reference, derived from transformations between 168 different image pairs. These are examined with respect to the coarseness of the deformation model employed.

Keywords: Spatial Normalisation, Inter-Subject Non-Rigid Registration, Brain Atlas, Normalised Mutual Information

1. INTRODUCTION

The ability to map volumetric brain image data from different subjects into a common reference space is becoming an increasingly valuable tool in all areas of brain imaging.[1–3] It allows direct voxel by voxel comparison of measurements made in each subject's anatomy and the construction of statistical maps of these measurements acquired from different clinical groups. However, the task of mapping different individual brains to a common space is a fundamental problem stemming from the inherent variability of human brain anatomy, particularly in the cortex.[4–6] The field of inter-subject brain mapping or atlas matching is extensive. It can be broadly divided into approaches attempting only to recover gross anatomical correspondence[7–9] (accounting for the size and shape of lobes etc), allowing analysis of residual structural differences,[10] and approaches which attempt to derive a complete voxel level correspondence between all smaller structures.[11–15] These finer, voxel level, estimation schemes have tended to focus on intensity based registration, rather than more sparse, feature based alignment. To deal with the problem of correspondence and missing or additional sulci or gyri, workers have examined the introduction of additional constraints into the volume registration process. These often make use of explicitly identified surfaces[16] or common sulci or gyri.[17,18] Other methods still, have looked at employing alternative coordinate systems, particularly the cortical surface, in which to carryout or refine the sulcal alignment.[2,19,20] However the extraction of specific features can be at the cost of providing a less automated solution, often requiring user interaction in the process of surface delineation in noisy or motion-corrupted data.

Within our research group, large scale clinical imaging studies are carried out on a range of degenerative brain diseases using both high resolution, multi-echo anatomical MRI and low resolution MRSI acquisitions. These diseases can commonly induce both atrophy and tissue contrast changes with respect to normal anatomy. We aim to develop a system capable of bringing all data from control and disease groups into a common reference space for analysis. Due to the large quantity of data and the variety of disease effects influencing tissue contrast, we have concentrated on developing fully automated techniques using voxel based rather than feature based registration. Here we examine the use of an entropy driven spatial normalisation scheme which may also provide robustness to local tissue contrast changes.

Further author information: (Send correspondence to C.S.)
C.S.: E-mail: cs1@itsa.ucsf.edu

2. METHODS

2.1. Registration criteria

Entropy derived alignment criteria such as joint entropy[21] and mutual information[22–25] have been shown to provide a robust measure of multi-modality alignment, while normalisation of the criteria provides further robustness through overlap invariance.[26] Although extreme intensity distortion has been shown to influence the registration measure requiring additional spatial encoding schemes,[27,28] this problem generally arises only for the most extreme intensity inhomogeneity induced by surface or phased array imaging coils. Here we make use of the overlap invariant form of normalised mutual information which can be expressed as,

$$\mathcal{C}(M_1; M_2) = \frac{H(M_1) + H(M_2)}{H(M_1, M_2)}, \tag{1}$$

where $H(M_1)$ and $H(M_2)$ are the marginal entropies of the reference $m_1 \in M_1$ and subject $m_2 \in M_2$ MRI values occurring in the volume of overlap of points,

$$\mathcal{X}_1' : \mathbf{x}_1 \in \mathcal{X}_1 | \mathbf{T}_{12}(\mathbf{x}_1) \in \mathcal{X}_2, \tag{2}$$

in the reference $\mathcal{X}_1$ and test subject $\mathcal{X}_2$ MRI volumes, related by transformation $\mathbf{T}_{12}$. $H(M_1, M_2)$ is the joint entropy of the co-occurrence of the values in the two scans. These entropies are evaluated from the joint probability distribution of corresponding image intensities $p(m_1, m_2)$ directly using,

$$H(M_1, M_2) = \sum_{m_1 \in M_1} \sum_{m_2 \in M_2} -p(m_1, m_2) log(p(m_1, m_2)), \tag{3}$$

$$H(M_1) = \sum_{m_1 \in M_1} -p_1(m_1) log(p_1(m_1)), \tag{4}$$

and,

$$H(M_2) = \sum_{m_2 \in M_2} -p_2(m_2) log(p_2(m_2)), \tag{5}$$

where,

$$p_1(m_1) = - \sum_{m_2 \in M_2} p(m_1, m_2), \tag{6}$$

and,

$$p_2(m_2) = - \sum_{m_1 \in M_1} p(m_1, m_2). \tag{7}$$

In our implementation, the joint probability distributions $p(m_1, m_2)$ are derived from a discrete histogram, evaluated for a given transformation, using tri-linear intensity interpolation.

2.2. Reference MRI atlas preparation

There are a number of approaches to constructing a common reference anatomy as a target for spatial normalisation. A popular approach is to use a single anatomy pre-aligned in standard coordinates,[29] allowing the reporting of the location of any findings in these standard coordinates. Alternatively an average brain can be constructed in an average coordinate system[8,15] to provide a reference anatomy which represents average of the variability of the group or groups being studied. However this process inherently depends on the basic step of inter-subject registration in order to create an average space. For this work, we examine the basic step of mapping between individual MRI's and make use of a single representative MRI as reference space. We are primarily concerned with accurate normalisation of different subject groups, rather than in the ability to report results in a standard anatomical coordinate system. The use of a single MRI as opposed to an averaged and blurred MRI ensures that we retain the finest anatomical structures for registration.

To improve the robustness to head and scalp shape variation and minimize computation time, we take a similar approach to that of[30] and make use of a brain editing step to limit deformation estimates to fitting only brain tissue defined in the atlas. The brain voxels are identified using a simple morphological segmentation requiring minimal

user interaction.[31] This step is only applied once to the reference atlas, and not to the MRI of each subject. All tissues outside the reference brain are set to a padding value to be ignored. MRI values of all tissues within the brain, including the CSF of the ventricles, are retained. A voxel dilation step is applied to retain a layer of between 2 and 4 voxels around the brain surface. This ensures that the outer boundary is included within the mask to aid in volume matching. This masked region is shown for the atlas data used in the experiments, in Figure 1.

2.3. Hierarchical transformation refinement

To provide a fully automated and robust estimate of the mapping between a subject and an atlas, we employ an hierarchical approach to the volume matching. This begins by estimating the rigid registration between a subject and the reference MRI using a multi-resolution optimization of Normalised Mutual Information.[26,25] We use the full MRI scan at this stage, rather than the brain masked reference image, to provide the most robust recovery of large scale alignment. This can automatically recover gross differences in patient positioning of 30 or more degrees, between a pair of scans.[26] We then further refine this global estimate by re-estimating a nine parameter (rigid and scale) transformation between the reference and subject anatomy. This is estimated using the brain masked reference image only, so that the scale estimates apply to the brain tissue only, and not the scalp, skull or other head features. This nine parameter global estimate then forms the starting point for the local-registration.

We have used an approach developed from those described in,[32,30,33] employing a smooth cubic B-Spline model for the geometric transformation field. This is controlled by a 3D lattice of control knots,

$$\mathbf{K}_{i,j,k} = \begin{pmatrix} \alpha_{i,j,k} \\ \beta_{i,j,k} \\ \gamma_{i,j,k} \end{pmatrix}, \tag{8}$$

at locations $(i,j,k) \in \mathbf{Z}^3$, to describe the B-spline[34] deformation in each axis. We distribute these regular lattice points with isotropic spacing of c voxels, over the the reference MRI such that $[i,j,k]^T.c \in \mathcal{X}_1$.

2.4. Estimation of fine lattice deformations using Normalised Mutual Information

We have modified the tissue deformation algorithm used in[30] in two important areas, to allow the estimation of much finer lattice deformation estimates between different brain anatomy.

The first issue in the estimation of finer lattice deformations using entropy measures, is that of limited statistical support for numerical derivative estimation. Using a histogram of say 64 by 64 bins, as in,[30] combined with a smaller region of support for each parameter, means that the numerically estimated change in the distribution $p(m_1, m_2)$, for a given change in parameter $\mathbf{K}_{i,j,k}$, is derived from very few voxel pairs. Depending on the structures present in a given region, the resulting change in the numbers of voxel value pairs contributing to each bin of a 64 by 64 histogram as a local region of image is deformed, can be very small. A direct approach to increasing the sensitivity of a histogram estimate of $p(m_1, m_2)$, is to increase the bin width. This is equivalent to extending the Gaussian window width in a parzen window estimate of the distribution. As discussed in,[35] we must be careful to ensure contrast between tissue regions providing registration information is retained in these binned or grouped intensities. For this application we are most concerned with the gray, white and CSF structures in the T1 MRI acquisition, stored as 8 bit numbers. We have therefore increased the bin width, reducing the total number of bins over the full range of MRI values to 24. Experimentally this visually maintains adequate contrast between the main tissues of interest in our T1 weighted 3D gradient echo acquisitions.

The second issue is the problem of retaining stability of the transformation estimate where there is no local image structure to determine the transformation parameter. Although B-Spline's have an inherent smoothness constraint, where groups of neighbouring control knots have no image structure to determine their value, folding of the transformation may still occur, as partial derivatives of the registration criteria are dominated by image noise. An example of such regions are those uniform areas of white matter below the cortex and around the ventricles. These are particularly a problem since they are also where large deformations can occur to accommodate significant differences in ventricle size in ageing or atrophied brains. Experimentally we have found that, unlike the use of coarser B-Spline brain deformation models,[30] folding does occur as the lattice spacing is decreased in inter-subject

registration. To prevent this, we have introduced an additional regularization term into the registration criteria. We have used the following bending energy,

$$\mathcal{B}(\mathbf{T}_{12}) = \frac{1}{N}\int_{x_1}\int_{x_2}\int_{x_3}\left[\left(\frac{\partial^2\mathbf{T}_{12}}{\partial x_1^2}\right)^2 + \left(\frac{\partial^2\mathbf{T}_{12}}{\partial x_2^2}\right)^2 + \left(\frac{\partial^2\mathbf{T}_{12}}{\partial x_3^2}\right)^2 + \left(\frac{\partial^2\mathbf{T}_{12}}{\partial x_1 x_2}\right)^2 + \left(\frac{\partial^2\mathbf{T}_{12}}{\partial x_2 x_3}\right)^2 + \left(\frac{\partial^2\mathbf{T}_{12}}{\partial x_1 x_3}\right)^2\right] dx_1 dx_2 dx_3, \tag{9}$$

evaluated and averaged over the N overlapping voxels in the reference MRI. This was employed by Ruckert et al[32,36] for a coarser 10mm B-Spline model of tissue deformation in the breast. Incorporating this into the global registration criteria gives the following expression:

$$\mathcal{R}(\mathbf{T}_{12}) = \mathcal{C}(\mathbf{T}_{12}) - w\mathcal{B}(\mathbf{T}_{12}), \tag{10}$$

to be maximised, where $\mathcal{C}(\mathbf{T}_{12})$ is the normalised mutual information between two MRI images evaluated for transformation $\mathbf{T}_{12}$ and w is the weighting term controlling the influence of the regularization to maintain smoothness of the transformation. The value of w was estimated experimentally on brain images to minimize folding conditions and remains fixed for all registrations presented here.

2.5. Evaluation and optimisation of the non rigid transformation

One of the main advantages for using a B-Spline model in our application in favor of other representations such as the thin-plate spline,[37] is the local nature of the control.[38] Since the deformation at a given location is determined only by the $4 \times 4 \times 4$ control knots around that point, moving any one control point affects only the location of $3c \times 3c \times 3c$ voxels lying around that point. This allows efficient evaluation of the partial derivatives of the global match criterion with respect to each spline control point location.

Following this initial global registration estimation procedure, the local B-Spline parameters $\mathbf{K}_{i,j,k}$ are initialised with the nine parameter (6 rigid + 3 scale) global transformation $\check{\mathbf{T}}_{12}$. Given that a third order B-Spline will pass through the control knot locations for a linear function, the control knots are simply initialised such that

$$\mathbf{K}^0_{i,j,k} = \check{\mathbf{T}}_{12}\left(\begin{bmatrix} i \\ j \\ k \end{bmatrix} c\right). \tag{11}$$

In order to find the deformation transformation we use a simple gradient ascent to find the maximum of the registration criteria. For each iteration we first estimate numerically the gradient vector $\nabla\mathcal{R}(\mathbf{K}_{i,j,k})$, of the *global* registration criteria with respect to each B-Spline parameter. The partial derivative components of knots for which the region of support does not fall 50% within the segmented and dilated brain volume are not evaluated but set to zero. The estimate of $\mathbf{K}^\iota_{i,j,k}$ at iteration ι is then updated in a simple up-hill search,

$$\mathbf{K}^{\iota+1}_{i,j,k} = \mathbf{K}^\iota_{i,j,k} + \lambda\nabla\mathcal{R}(\mathbf{K}^\iota_{i,j,k}). \tag{12}$$

The initial value of λ was found experimentally and the same initial value was used for all registrations in this paper. An adaptive reduction in λ was used so that the rate of ascent is reduced such that $\lambda \mapsto \lambda/2$ when $\mathcal{R}(\mathbf{K}^{\iota+1}) \leq \mathcal{R}(\mathbf{K}^\iota)$. A multi-grid approach derived from that described in[30] is used to provide an efficient and robust recovery of larger scale deformations. However, the range of deformations between one individual anatomy and another, ranging from the size of overall lobes down to differences in the thickness of the gray matter layer in the cortex is appreciably greater than that induced by physical brain tissue deformation. To estimate this much larger dynamic range of deformations we have used a pyramid of B-Spline lattices with four levels and a factor two between the lattice spacing in each. The deformation lattice spacing and the underlying image resolution used to estimate the deformation is directly linked: the base resolution of the MRI's is set by re-sampling both MRI images to 0.8mm cubic voxels using a Gaussian filtering kernel of 0.8mm F.W.H.M. The base resolution of the deformation lattice is set to 3 voxels or 2.4mm. Up from this base level, the image sampling resolution and spatial resolution is reduced by a factor 2 as the lattice and voxel spacing is increased by a factor of two at each level. The four image resolutions aligned in order are 6.4mm, 3.2mm, 1.6mm and 0.8mm, using lattices of spacing 19.2mm, 9.6mm, 4.8mm and 2.4mm respectively.

Starting at the coarsest resolution, the optimisation is run to convergence at each level. The convergence criteria is simply based on the percentage change in the criteria falling below a set level. This was determined experimentally and fixed at 0.0025% for each level except the finest 2.4mm knot spacing which is allowed to converge down to a percentage change of less than 0.0002%.

2.6. Test data

All data used in these experiments was acquired in imaging studies carried out within MRI unit at the V.A.M.C. in San Francisco. We focused on the use of high resolution 3D gradient echo T1 weighted anatomical MRI images which were acquired on a Siemens Vision system, using an MPRAGE sequence (TR=10ms,TE=4ms). The images were reconstructed with a voxel size of $1mm \times 1mm \times 1.5mm$.

2.6.1. Choice of reference anatomy

In the general case, for most of these studies, one or more groups of healthy subjects with given demographics (age,sex,handedness,etc) are imaged to form a reference for MRI and MRSI measurements. One or more groups of disease subjects are then also imaged and comparisons made between groups. It is assumed that a normal or control anatomy will be used as a reference space for any analysis. One of the major variables affecting anatomy between normal controls is the age of the group being studied. Depending on the clinical condition being studied the imaging may concentrate on an older group only (for example in Alzheimer's imaging) or have a range of ages (for example in the study of the effects of alcohol). We have therefore selected two data sets with significantly different ages to be used as target anatomies to compare spatial normalisation of different groups. These two MRI's are shown in brain masked form in Figure 1.

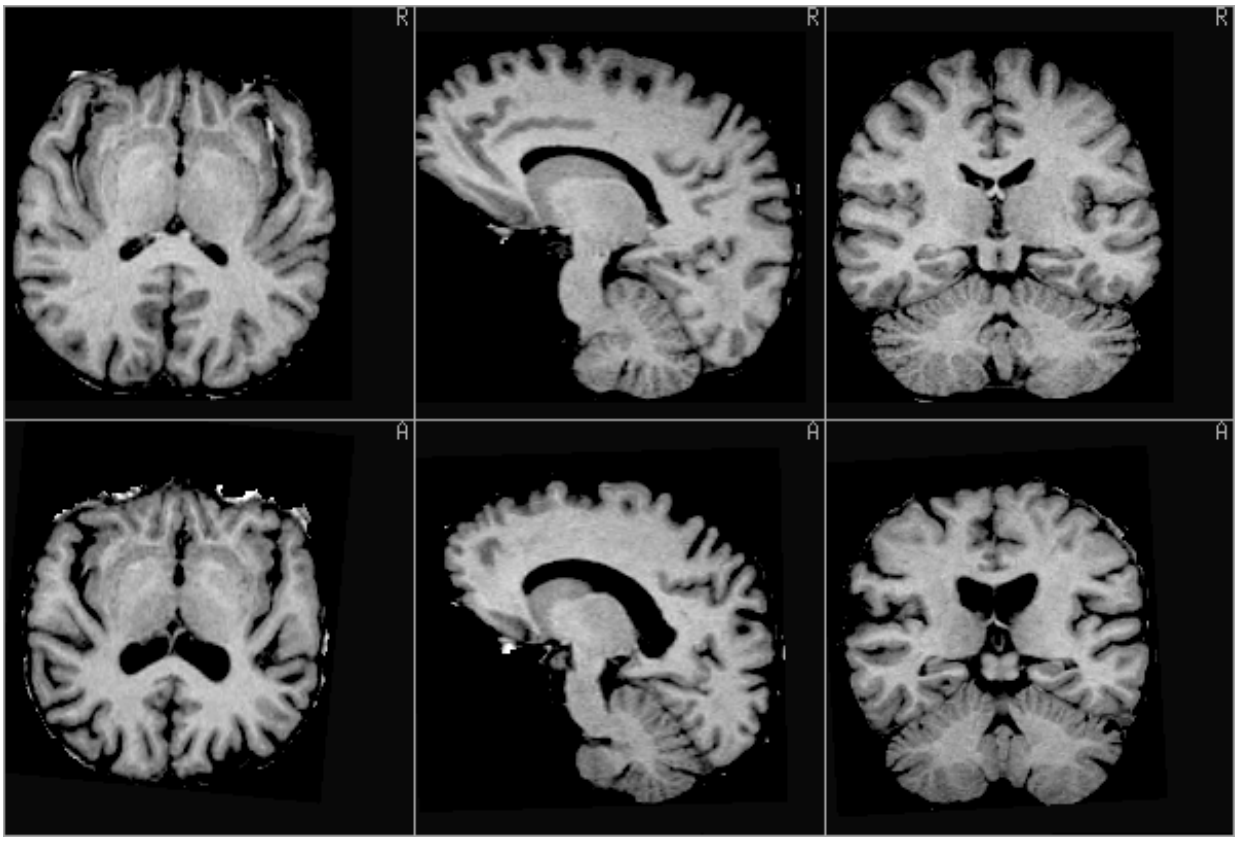

Figure 1. Orthogonal slices through the MRI data sets used as a target reference spaces: Top row shows the 33Y/old male used as a younger reference anatomy. The bottom row shows the 72 Y/old female used as the older reference anatomy. Note differences in the size of the ventricles and the sulcal C.S.F. spaces.

2.6.2. Selection of test groups

Three test groups were selected to represent the range of data being acquired in our clinical studies. These consisted of a group of younger normal subjects (N=16, mean age=33yrs, all male), a group of older normal subjects (N=16,mean

age=68yrs,6 male, 10 female), and a group of older probable Alzheimer's patients (N=10, mean age=79yrs, 5 male, 5 female).

3. EXPERIMENTAL RESULTS

3.1. Spatial alignment of image intensities

Following estimation of the transformation of each subject in each group to each of the two reference MRI's, each subject MRI was transformed into the coordinate system of the reference MRI using tri-linear intensity interpolation. To investigate the effect of the B-Spline knot spacing, this was done using each of the four levels of knot spacing. The average image was then calculated for each spatially normalised group. The average images for the young normal control group are shown in Figure 2, using all four lattice spacings. The blurring of the average image resulting from misalignment of structures across the different subjects is clearly visible in the coarser deformation models. As the lattice spacing is reduced, the smaller sulci and gyri are revealed within this average image. This focusing is particularly apparent in the sagittal slice.

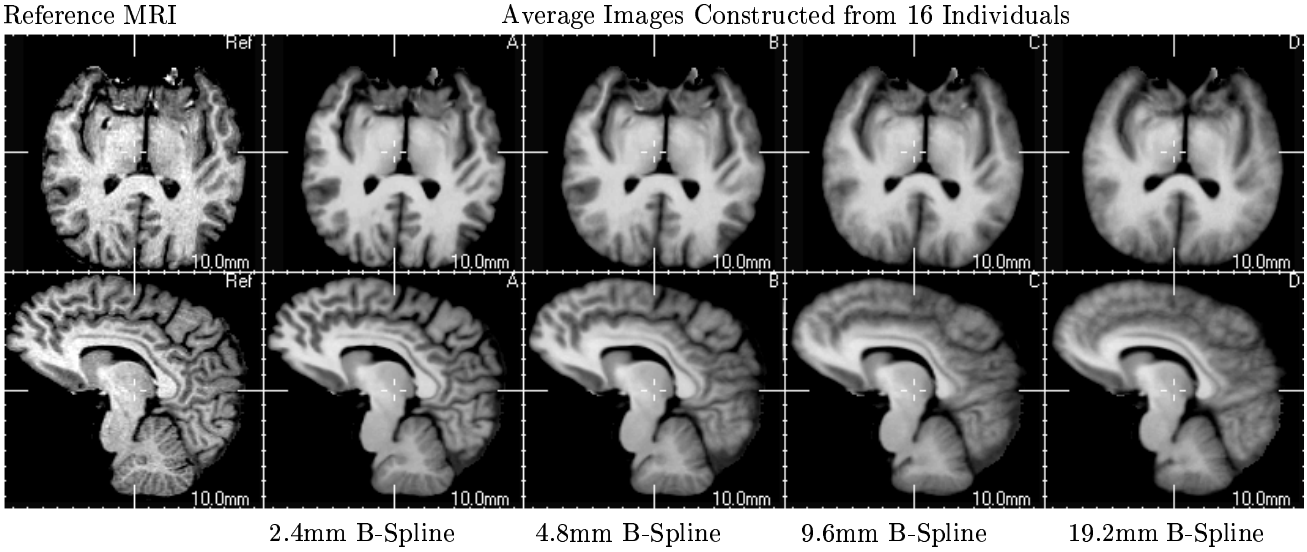

Figure 2. Transaxial (top) and sagittal (bottom) slices through the young normal reference MRI (left) and average images created from the 16 spatially normalised MRI's of the young normal group. The four average images were created using transformation estimates provided by the different levels of B-Spline lattice spacing, shown below each image in mm. The improvement in alignment is most clearly seen in the smaller sulci of the cortex. (All image data shown with an identical mapping from MRI to gray value)

For comparison, Figure 3 shows the average image calculated from each of the younger control, older control and Alzheimer's groups mapped to the younger reference MRI using the solution from the finest deformation lattice. The older and younger group averages are very similar, down to the finer cortical structures. However, from closer inspection of the sagittal slice in the Alzheimer's average image, it is clear that there is a darkening and loss of finer sulcal structures. This suggests the presence of a residual disease related atrophy in the spatially normalised average scan, which is not captured by our 2.4mm B-Spline deformation estimate.

We then investigated how well the entropy criteria, combined with the deformation model is aligning intensities in the different subjects. To do this we evaluated the mean standard deviation of the MRI intensity at each point in the reference space, across the masked brain voxel values of the normalised MRI's. This was repeated for each group, each reference MRI and each B-Spline lattice spacing. These averaged standard deviations are shown as plots against lattice spacing in Figure 4. These traces indicate that the ability of the spatial normalisation simply to align intensity values, is clearly influenced by the choice of reference anatomy. Fewer residual intensity differences are seen when mapping a younger group to a younger reference brain, than when mapping the same group to an older

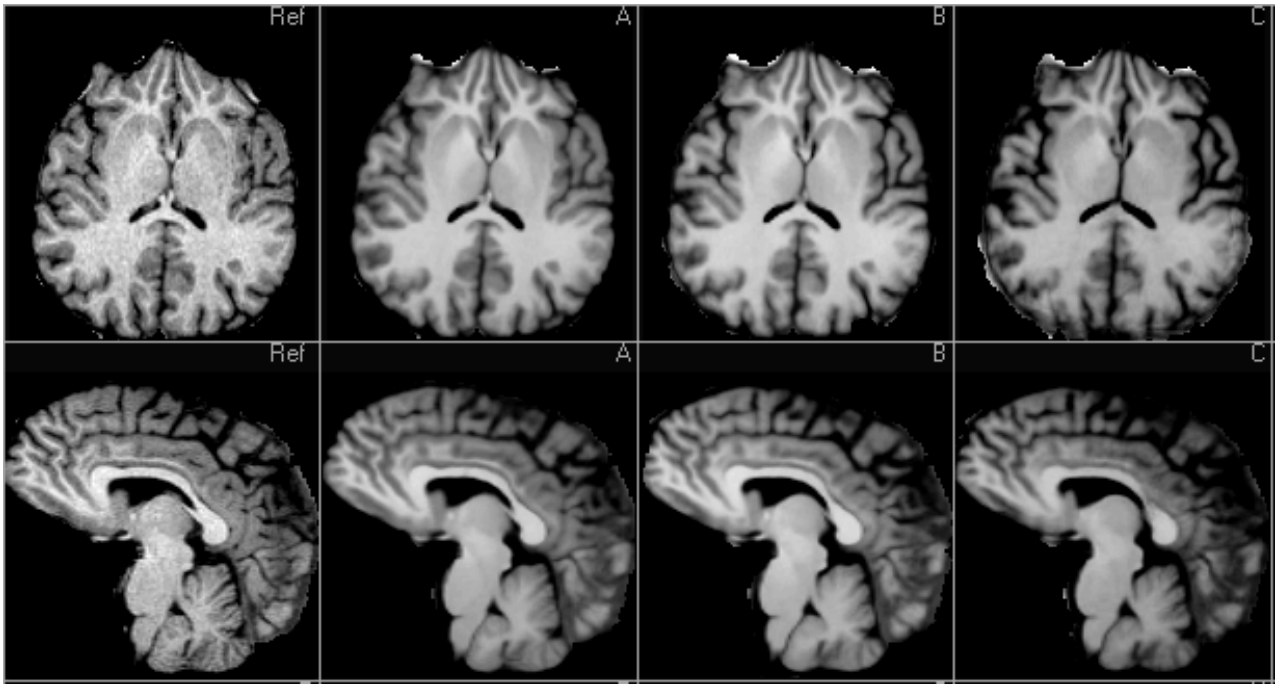

Figure 3. Transaxial (top) and sagittal (bottom) slices through the young normal reference MRI (left) and average images created from the spatially normalised MRI's of the young normal group, older normal group and the Alzheimer's group. (All image data shown with an identical mapping from MRI to gray value)

reference brain. For the older normal control group however, the use of either reference MRI appears to provide comparable recovery of intensity alignment. The largest sensitivity to choice of reference anatomy is seen in the older Alzheimer's group. Here the use of a younger reference atlas appears to significantly degrade the alignment of MRI values when compared to using a reference MRI from an older individual.

Overall, the consistant reduction in residual intensity variation as the deformation lattice spacing is reduced, indicates that, at least in some parts of the image, the transformation model is still under fitting to the true anatomical mapping.

3.2. Spatial discrepancy in anatomical transformations

Our aim is to investigate the spatial distribution of errors when estimating the mapping between a group of subjects and a given reference anatomy. Without a voxel by voxel ground truth defining the correspondence from individual to reference for each subject, the error cannot be directly measured. However, we can examine the consistency or precision of this mapping by comparing multiple registration estimates. The approach we have taken is illustrated in Figure 5. We use R to denote a reference anatomy, and let S1 and S2 denote subjects 1 and 2 from the same group, G. $\mathbf{T}_{R1}$ and $\mathbf{T}_{R2}$ describe the transformations from the reference to S1 and S2. Let $\mathbf{T}_{12}$ be an additional transformation from S1 to S2. Each transformation $\mathbf{T}_{ij}$ has some immeasurable error ϵ_{ij} with mean μ_{ij} and variance σ_{ij}^2.

Consider a point $\mathbf{x}_R$ in reference space. Let $\mathbf{x}_2$ be the same point after transformation into subject S2 using $\mathbf{T}_{12}\mathbf{T}_{R1}\mathbf{x}_R$, and let $\mathbf{x}_{2\prime}$ be the point transformed in subject S2 using $\mathbf{T}_{R2}\mathbf{x}_R$. Because each $\mathbf{T}_{ij}$ has some error, in general $\mathbf{x}_2 \neq \mathbf{x}_{2\prime}$, and ϵ_{GA} denotes the discrepancy between $\mathbf{x}_2$ and $\mathbf{x}_{2\prime}$. We assume that the transformation $\mathbf{T}_{ij}$ is smoothly varying and can be approximated locally by a linear model, so that for small errors we have:

$$\epsilon_{GA} = \epsilon_{R1} + \epsilon_{R2} + \epsilon_{12}. \tag{13}$$

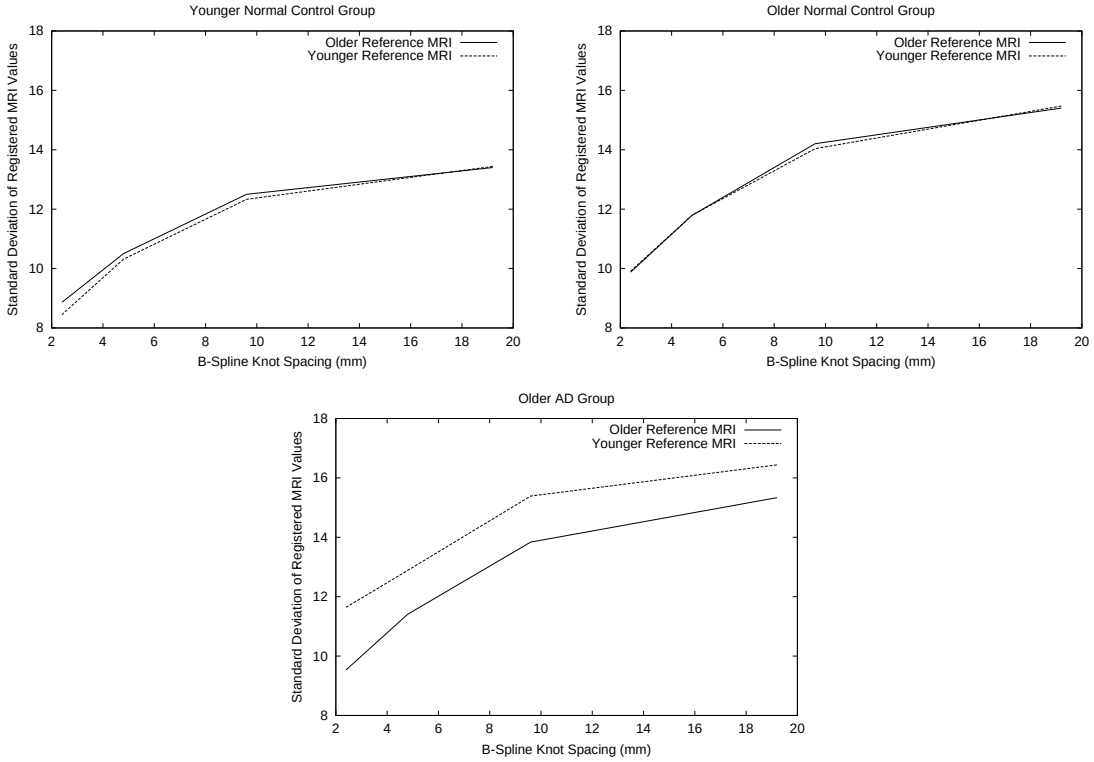

Figure 4. Graphs showing the relationship between the residual intensity variation after registration for each group of MRI's to each reference MRI, using different B-Spline knot spacing's.

If independence of the transformations and errors are also assumed,[39] then the mean and variance of the error at that point over a group of subjects can be estimated as,

$$\mu_{GA} = \mu_{R1} + \mu_{R2} + \mu_{12} \tag{14}$$

$$\sigma^2_{GA} = \sigma^2_{R1} + \sigma^2_{R2} + \sigma^2_{12}. \tag{15}$$

The quantities μ_{GA} and σ^2_{GA} can be estimated for each group of subjects. We can assume that $\mu_{RG} := \mu_{R1} \approx \mu_{R2}$ and $\sigma^2_{RG} := \sigma^2_{R1} \approx \sigma^2_{R2}$, where μ_{RG} and σ^2_{RG} are the mean and variance of the error of transformation from the reference into the subject group. If additional within group registrations are performed, then we can obtain an estimate of μ_{12} and σ^2_{12} as follows. As shown in Figure 5, let S3 denote subject 3 from group G, and let $\mathbf{T}_{23}$ and $\mathbf{T}_{13}$ describe the transformations from S2 and S1 to S3. Consider a point $\mathbf{x}_1$ in subject S1. Let $\mathbf{x}_3$ be the same point after transformation into subject S3 using $\mathbf{T}_{23}\mathbf{T}_{12}\mathbf{x}_1$, and let $\mathbf{x}_3\prime$ be the point transformed into subject S3 using $\mathbf{T}_{13}\mathbf{x}_1$. Because of the transformation errors, generally $\mathbf{x}_3 \neq \mathbf{x}_3\prime$, and ϵ_{GG} denotes the distance between these points. Using the same linearity assumption as before, we have,

$$\epsilon_{GG} = \epsilon_{12} + \epsilon_{23} + \epsilon_{13}, \tag{16}$$

and assuming independence of the transformations and errors, the mean and variance are,

$$\begin{aligned} \mu_{GG} &= \mu_{12} + \mu_{23} + \mu_{13} \\ \sigma^2_{GG} &= \sigma^2_{12} + \sigma^2_{23} + \sigma^2_{13}. \end{aligned} \tag{17}$$

The quantities μ_{GG} and σ^2_{GG} can be estimated for each group of subjects. If we assume that $\mu_w := \mu_{12} \approx \mu_{23} \approx \mu_{13}$ and $\sigma^2_w := \sigma^2_{12} \approx \sigma^2_{23} \approx \sigma^2_{13}$, where μ_w and σ^2_w are the mean and variance of the error of transformation within a

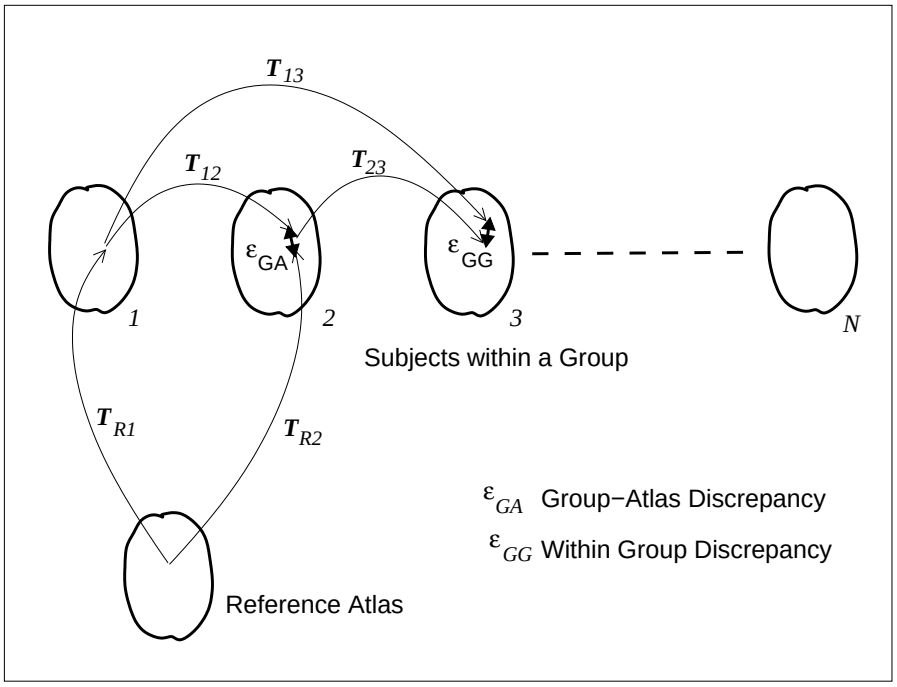

Figure 5. An illustration of the estimation of within and between group discrepancy using combinations of multiple transformation estimates.

subject group, then we can let $\mu_w = \mu_{GG}/3$ and $\sigma_w^2 = \sigma_{GG}^2/3$. These estimated quantities can be substituted for μ_{12} and σ_{12}^2 in equations 14 and 15, along with μ_{RG} and σ_{RG}^2 we get,

$$\begin{aligned} \mu_{GA} &= 2\mu_{RG} + \mu_w \\ \mu_{GA} &= 2\mu_{RG} + \mu_{GG}/3 \\ \mu_{RG} &= \frac{\mu_{GA} - \mu_{GG}/3}{2}, \end{aligned} \tag{18}$$

Different groups of subjects can be registered to different reference anatomies, and the estimates of μ_{RG} can be calculated at each point $\mathbf{x}_R$ in the reference anatomy, in order to determine the degree to which the choice of reference influences the precision of the resulting registration.

Transformation estimates between a total of 168 different image pairs were calculated (each scan of each group was registered to each reference MRI, its neighbour in the group and its next neighbour, as in Figure 5). For each of the groups and reference MRI's, the mean value of μ_{RG} was estimated over the entire segmented reference brain. These results are summarised in table 1. From these it is clear that, as with the intensity variation, the choice of reference anatomy influences the precision of the final registration estimates. The younger control group of MRI scans appear to be aligned with comparable precision to both the younger and older reference MRI. This may be because this group is simply more limited in the range of anatomical variation, particularly in the shape and size of the ventricles and sulcal spacing, compared to the older groups, and therefore requires a less extreme range of deformations. The older normal and older Alzheimer's groups are however more consistently mapped to the older reference MRI, than the younger reference MRI. There is though, little difference in the consistency between the mapping of the older Alzheimer's and the older normal control group to the older atlas. In fact, the older reference MRI appears to be a slightly better match to the Alzheimer's group, than to the older normal group. Overall, this comparable consistency in mapping from both the older groups to the older atlas is important, since it allows us to use this older reference as a common space in the comparison of structural or metabolite maps created from both groups.

The spatial distribution of these discrepancies was also examined. An example of the regions of greatest average

Ref.	Younger Group	Older Group	Older AD Group
Younger MRI	1.68mm	1.99mm	2.00mm
Older MRI	1.63mm	1.76mm	1.66mm

Table 1. Estimates of the mean discrepancy (μ_{RG}) in mapping points from reference MRI to subject MRI averaged over the reference MRI brain voxels.

discrepancy in mapping the older Alzheimer's group to the older reference MRI are shown by iso-discrepancy contours in Figure 6. From this it is clear that the main discrepancies occur in the outer cortex, presumably where single sulci in the reference MRI must map to multiple sulci in one of more of the subjects, or vice versa. Another interesting region of discrepancy in the Alzheimer's group transformation estimates occurs around the left (right in the coronal image) hippocampus. Given that this is a known site of atrophy in Alzheimer's disease this local region of discrepancy may be a function of disease, rather than normal variability.

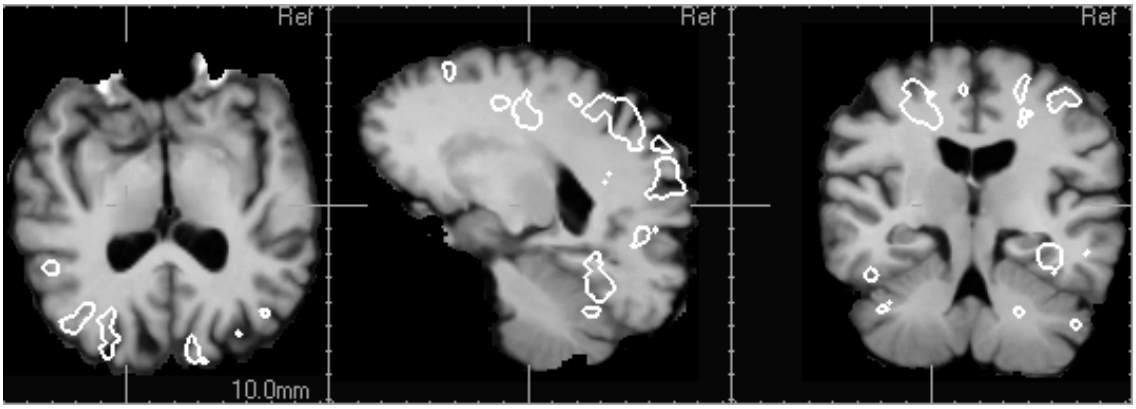

Figure 6. Transaxial, sagittal and coronal slices through the average AD group MRI in older reference MRI coordinates (2.4mm B-Spline transformation estimates), with an iso-discrepancy contour showing regions where the estimated average discrepancy in the reference to subject transformation exceeded 3mm (twice the slice thickness) over the 10 subjects.

4. DISCUSSION

We have developed a fully automated high resolution spatial normalisation methodology driven by Normalised Mutual Information, and examined its ability to consistently align a range of different types of brain anatomy to different reference anatomies. Estimation of a single transformation to the highest deformation resolution (2.4mm B-Spline knot spacing) takes between 2 and 4 hours on an 800Mhz Pentium III CPU, running a C++ implementation under the Linux operating system. High resolution B-Spline deformations were estimated between a total of 168 different image pairs, within three different subject groups. All registration estimates in this study were carried out completely automatically with no starting estimates or user intervention, other than the segmentation of brain anatomy from the two reference MRI's.

We evaluated the ability of the algorithm to bring different types of brain anatomy into registration with different reference MRI's in two ways. Firstly we examined the residual intensity variation across each group of subjects following spatial normalisation. These results indicated that the use of an older reference anatomy for spatial normalisation of older or atrophied brain anatomy appreciably decreased the residual intensity differences in the normalised MRI's. Secondly we examined the spatial discrepancy of the transformation estimates when registering the groups to different reference MRI's. These results again indicated that the ability to consistently map groups of subject brains to a reference MRI was influenced by the choice of reference anatomy.

The results we obtained in this work were certainly influenced by our choice of final lattice spacing. A finer B-Spline lattice spacing may have decreased the residual errors by allowing the thinning of gray matter layers in the atrophy group to be more fully described by the spatial normalisation. Our choice was mainly limited by computing resources (both memory and CPU), and we hope to gain more experience with finer scale deformation models when more powerful computing resources are available. However it may be the case that finer deformation models increase the effect of over-fitting and lead to an increase in the discrepancy of transformations elsewhere.

In this work we have concentrated on the influence of age and atrophy as the main confounding factors, since these are the main variables in many of our imaging studies. We have not however examined the influence of other demographic classifications such as sex or handedness. In the future we plan to extend the work to examine effect of these and other more varied clinical subject groups, where tissue contrast variation (rather than simply tissue loss) arising from disease may also be an important factor.

ACKNOWLEDGMENTS

This work was funded by a NIH grant P01 AG12435 and PO1 AA11493. The authors wish to thank D. Truran for helping select and prepare the atlas data, Dr B. Miller and Dr B. Jagust for access to imaging data and Dr L. Rogers for advice on the statistical analysis.

REFERENCES

1. K. Friston, A. Holmes, K. Worsley, J. Poline, C. Frith, and R.S.J.Frackowiak, "Statistical parametric maps in functional imaging: A general linear approach," *Human Brain Mapping* **2**, pp. 189–210, 1995.
2. P. Thompson, R. Woods, M. Mega, and A. Toga, "Mathematical/Computational challenges in creating deformable and probabilistic atlases of the human brain," *Human Brain Mapping* **9**, pp. 81–92, 2000.
3. U. Grenander and M. I. Miller, "Computational anatomy: An emerging discipline," *Quart. Appl. Math* **56**(4), pp. 617–694, 1998.
4. A. Bartley, D. Jones, and D. Weinberge, "Genetic variability of human brain size and cortical gyral patterns," *Brain* , pp. 257–269, 1997.
5. A. Galaburda, G. Rosen, and G. Sherman, "Individual variability in cortical organization: Its relationship to brain laterality and implications to function," *Neuropsychologia* , pp. 529–546, 1990.
6. K. Zilles, E. Armstrong, A. Schleicher, and H. Kretschmann, "The human pattern of gyrification in the cerebral cortex," *Anat. Embryol.* **179**, pp. 173–179, 1988.
7. K. Friston, J. Ashburner, C. Frith, J. Poline, J. Heather, and R. Frackowiak, "Spatial registration and normalisation of images," *Human Brain Mapping* **2**, pp. 165–189, 1995.
8. R. Woods, S. Grafton, J. Watson, N. Sicotte, and J. Mazziotta, "Automated image registration II: Intersubject validation of linear and non-linear models," *Journal of Computer Assisted Tomography* **22**, pp. 153– 165, 1998.
9. P. Kochunov, J. Lancaster, and P. Fox, "High speed spatial normalisation using an octree method," *NeuroImage* **10**, pp. 724–737, 1999.
10. J. Ashburner and K. Friston, "Voxel-based morphometry-the methods," *NeuroImage* **11**, pp. 805–821, 2000.
11. G. Christensen, R. Rabbitt, and M. Miller, "Deformable templates using large deformation kinematics," *IEEE Transactions on Image Processing* **5**, pp. 1435–1447, 1996.
12. D. Collins, A. Evans, C. Holmes, and T. Peters, "Automatic 3D segmentation of neuro-anatomical structures from MRI," in *Proceedings of Information Processing in Medical Imaging*, Y. Bizais, C. Barillot, and R. D. Paola, eds., pp. 139–152, Kluwer Academic Publishers, 1995. Brest, France.
13. J.-P. Thirion, "Image matching as a diffusion process: An analogy with maxwells demons," *Medical Image Anal.* **2**(3), pp. 243–260, 1998.
14. M. Bro-Nielsen and C. Gramkow, "Fast fluid registration of medical images," in *Proceedings of the 4th International Conference on Visualization in Biomedical Computing*, K. Hohne and R. Kikinis, eds., pp. 267–276, Springer-Verlag, 1996.
15. T. Schormann, S. H. A. Bürgel, K. Engler, and K. Zilles, "A new technique for 3-D nonlinear deformation: Application to studies of the variability of brain structures," *NeuroImage* , p. S418, 1997.
16. C. Davatzikos, "Spatial transformation and registration of brain images using elastically deformable models," *Comp Vision and Image Understanding* **66**(2), pp. 207–222, 1997.

17. D. Collins, G. Goualher, R. Venugopal, A. Caramanos, A. Evans, and C. Barillot, "Cortical constraints for non-linear cortical registration," in *Proceedings of the 4th International Conference on Visualization in Biomedical Computing*, K. Hohne and R. Kikinis, eds., pp. 307–316, Springer-Verlag, 1996.
18. M. Vaillant and C. Davatzikos, "Hierarchical matching of cortical features for deformable brain image registration," in *Proc. Image Processing in Medical Imaging*, pp. 182–195, Springer Verlag, (Berlin), 1999.
19. B. Fischl, M. I. Sereno, R. B. Tootell, and A. Dale, "High-resolution intersubject averaging and a coordinate system for the cortical surface," *Human Brain Mapping* **8**, pp. 272–284, 1999.
20. P. Thompson and A. Toga, "A surface-based technique for warping magnetic resonance images of the human brain," *IEEE Transactions on Medical Imaging* **4**, pp. 402–417, 1996.
21. A. Collignon, D. Vandermeulen, P. Suetens, and G. Marchal, "3D multi-modality medical image registration using feature space clustering," in *Proceedings of the 1st International Conference on Computer Vision, Virtual Reality and Robotics in Medicine*, pp. 195–204, Spinger-Verlag, 1995. Nice.
22. W. Wells, P. Viola, H. Atsumi, S. Nakajima, and R. Kikinis, "Multi-modal volume registration by maximisation of mutual information," *Medical Image Analysis* **1**(1), pp. 35–51, 1996.
23. P. Viola and W. Wells, "Alignment by maximisation of mutual information," in *Proceedings of the 5th International Conference on Computer Vision*, pp. 15–23, 1995.
24. A. Collignon, F. Maes, D. Delaere, D. Vandermeulen, P. Suetens, and G. Marchal., "Automated multimodality image registration using information theory," in *Proceedings of Information Processing in Medical Imaging*, Y. Bizais, C. Barillot, and R. D. Paola, eds., pp. 263–274, Kluwer Academic Publishers, 1995. Brest, France.
25. C. Studholme, D. Hawkes, and D. L. G. Hill, "Robust fully automated 3D registration of MR and PET images of the brain using multiresolution voxel similarity measures.," *Medical Physics* **24**(1), pp. 25–35, 1997.
26. C. Studholme, D. Hill, and D. Hawkes, "An overlap invariant entropy measure of 3D medical image alignment," *Pattern Recognition* **32**(1), pp. 71–86, 1999.
27. C. Studholme, D. Hill, M.N.Maisey, and D. Hawkes, "Registration measures for automated 3D alignment of PET and intensity distorted MR images," in *Proceedings in Image Fusion and Shape Variability Techniques*, pp. 186–193, Leeds University Press, 1996.
28. C. Studholme, P. Summers, D. Hill, and D. Hawkes, "An information theory approach to the alignment of images containing measurement inhomogeneity: Application to MR surface coil angiography of the brain," in *Proceedings of Medical Image Understanding and Analysis*, pp. 45–48, Oxford University Press, 1997.
29. J. Talairach and P. Tournoux, *Co-Planar Sterotaxic Atlas of the Human Brain*, Thieme, New York, 1988.
30. C.Studholme, E. Novotny, I. Zubal, and J. Duncan, "Estimating tissue deformation between functional images induced by intracranial electrode implantation using anatomical MRI," *NeuroImage* **In Press**, 2001.
31. K. Höhne and W. Hanson, "Interactive 3D segmentation of MRI and CT volumes," *Journal of Computer Assisted Tomography* **16**(2), pp. 285–294, 1992.
32. D. Ruckert, C. Hayes, C. Studholme, M. Leach, and D. Hawkes, "Non-rigid registration of breast MR images using mutual information," in *Proceedings of MICCAI*, W. M. Wells, A. Colchester, and S. Delp, eds., pp. 1144–1152, 1998. Cambridge, MA, USA.
33. C. Studholme, R. T. Constable, and J. S. Duncan, "Accurate alignment of functional EPI data to anatomical MRI using a physics based distortion model," *IEEE Transactions on Medical Imaging* **19**(11), pp. 1115–1127, 2000.
34. S. Lee, G. Wolberg, K. Chwa, and S. Shin, "Image metamorphises with scattered feature constraints," *IEEE Transactions on Visualisation and Computer Graphics* **2**(4), pp. 337–354, 1996.
35. C. Studholme, *Measures of 3D Medical Image Alignment*. PhD thesis, University of London, 1997.
36. D. Ruckert, L. Sonoda, C. Hayes, M. Leach, and D. Hawkes, "Nonrigid registration using free-form deformations: Application to breast MR images," *IEEE Trans. Med. Imaging* **18**(8), pp. 712–721, 1999.
37. C. Meyer, J. Boes, B. Kim, P. Bland, K. Zasadny, P. Kison, K. Koral, K. Frey, and R. Wahl, "Demonstration of accuracy and clinial versatility of mutual information for automatic multimodality image fusion using affine and thin-plate spline warped geometric deformations," *Medical Image Analysis* **3**(1), pp. 195–206, 1997.
38. J. Foley, A. van Dam, S. Feiner, and J. Hughes, *Computer Graphics, Principles and Practice*, Addision Wesley, Mass. U.S.A., 1990.
39. R. Hogg and E. Tanis, *Probability and Statistical Inference*, Macmillan, New York, U.S.A., 1988.